The External Microbiome Communicates with the Developing Zebrafish (*Danio rerio*) Embryo Through the Protective Chorion and Influences Developmental Trajectory

[1]Green, Emily, [1]Harishchandra, Akila, [1] Ranasinghe, Prabha, [1]Di Giulio, Richard, [1]Jayasundara, Nishad

[1]Nicholas School of the Environment, Duke University, Durham, NC 27708, USA
emily.green@duke.edu

Abstract

The commensal microbiome plays a significant role in shaping host physiological processes including energy metabolism and neurobiology. However, current knowledge on host-microbiome interactions is limited to effects of the microbiome during post-embryonic development. Elucidating mechanisms and consequences of host-microbe communication during embryonic development, particularly in oviparous organisms is a notable gap. Protected from the chorionic fluid and considered to be sterile, embryonic development in oviparous organisms is typically considered to be independent of the influence of the microbiome. Here, we tested the hypothesis that the external microbiome influences embryonic development in oviparous organisms despite lack of physical contact. We utilized zebrafish (*Danio rerio*) reared germ-free (GF) and conventionalized with microbes (CV) at different times during embryonic development to examine changes in the embryonic transcriptome, proteome, and physiology during embryogenesis at 32 hours post-fertilization. Our results contrast the conventional notion that zebrafish embryos are shielded from the external microbial environment by their protective chorion until hatching. We demonstrate the external microbial community influences embryonic transcript and protein abundance associated with critical developmental processes including energy metabolism and neurodevelopment. While these pathways are previously identified to be influence by microbes during *post*-embryonic stages, here, we reveal a significant role of the surrounding aquatic microbial community in regulating these processes as early as embryogenesis. Furthermore, we demonstrate the external microbial community differentially regulates cytochrome P450 driven xenobiotic metabolism and associated bioenergetic and behavioral responses following exposure to a CYP1A activator during embryogenesis. These findings transform our interpretation and consideration of embryonic development as a function of microbial cues and genetic blueprints, enhance knowledge of fundamental processes governing vertebrate embryonic development, and expand comprehension of host-microbe communication.

1. Introduction

Eukaryotic evolution occurred in an environment abundant with microorganisms, resulting in co-evolved symbiotic relationships between multi-cellular organisms and microbes (McFall-Ngai et al., 2013). It is well established that the commensal microbiome, an ecosystem teeming with trillions of microorganisms, is critical to maintain optimal vertebrate physiological processes including immune function, digestion, xenobiotic response, behavior, and energy metabolism (Bertotto et al., 2020; Catron et al., 2019; Cholan et al., 2020; Davis et al., 2016; Gómez & Balcázar, 2008; Heijtz et al., 2011; McFall-Ngai et al., 2013; Neis et al., 2015; Phelps et al., 2017; Sampson & Mazmanian, 2015; Venema, 2010). Furthermore, evidence indicates the commensal microbiome may modulate vertebrate development (McFall-Ngai et al., 2013). For example, metabolic homeostasis during post-embryonic development is influenced by the gut microbiome. Microbial metabolites, such as short-chain fatty acids (SCFA), can mediate post-embryonic energy homeostasis by binding to G-protein coupled receptors (GPCRs) on epithelial cells, exerting a downstream influence on lipid, glucose, and ATP metabolism (Brown et al., 2003; Den Besten et al., 2013; Gao et al., 2009). Furthermore, current studies investigating the bidirectional communication of the gut-brain axis during post-embryonic development reveal microbes and their products transmit signals from the gut to the brain via various mechanisms including the vagus nerve, binding to GPCRs on afferent nerves, or entering systemic circulation and traversing the blood brain barrier (Brown et al., 2023; Davis et al., 2016; Kimura et al., 2013; MacFabe, 2012; Martin et al., 2018; Sampson & Mazmanian, 2015; Silva et al., 2020). These findings exemplify the profound integration of critical post-embryonic developmental processes with microbial-directed signals and cues, emphasizing the importance of a healthy microbiome throughout development. However, this predominant focus on *post*-embryonic development highlights a significant gap in our understanding of host-microbe relationships during embryogenesis, when organisms are highly susceptible to changes in developmental trajectory.

During embryogenesis, developmental trajectory is highly sensitive to the external environment, emphasizing the importance of understanding the effects of the microbial community during early-life development (Hamdoun & Epel, 2007; Wilson, 1973). Egg-laying oviparous organisms are exposed to an abundant and diverse microbial ecosystem, full of both mutualistic and pathogenic bacteria, during early development. Therefore, many organisms evolved defense strategies to protect the developing embryo from the external environment, including microbes, during critical periods of sensitivity (Hamdoun & Epel, 2007). Some oviparous vertebrates develop inside an egg shell barrier or receive antimicrobial peptides via maternal transfer during egg deposition, shielding the embryo from pathogenic infections that could hinder development (Benkendorff et al., 2001; De La Paz et al., 2020; Wang et al., 2012; Wang & Zhang, 2010; Wilkins et al., 2015, 2016). For example, in zebrafish (*Danio rerio)* embryos develop in a three-layer acellular chorion, perforated with small pore canals spanning 0.5-0.78μm in diameter, essential for internal transport of oxygen and nutrients while restricting entry of larger molecules such as microbes (Chen et al., 2020; Pham et al., 2008; Phelps et al., 2017; Rawson et al., 2000). As microbes are too large to physically breach the chorionic barrier, conventional knowledge is that vertebrate embryos, including zebrafish, are shielded from the microbial environment until hatching (Pham et al., 2008; Phelps et al., 2017).

Despite the notion that microbes are too large to physically breach the chorion, evidence highlights that external bacterial diversity can affect hatching and survival rates, as well as provide protection against predation and pathogenic invasion during embryonic development (Kellner, 2002; Kellner & Dettner, 1996; Martín-Vivaldi et al., 2014; Wedekind, 2016; Wilkins et al., 2016). Due to the beneficial effects, some vertebrates selectively recruit microbes to the exterior surface of the embryo for protection (Flórez et al., 2015; Hamdoun & Epel, 2007; Phelps et al., 2017), although the mechanisms in which these external microbial communities affect embryonic development and the associated developmental outcomes remain understudied. Two studies have demonstrated microbial effects in isolated brain and cranial regions in developing embryos (Rea et al., 2022; Vuong et al., 2020). In humans, research demonstrates the maternal microbiome influences fetal health and pregnancy outcomes (Pelzer et al., 2017; Vuong et al., 2020; Younge et al., 2019; Zakis et al., 2022). However, the mechanisms in which microbes impact *in utero* development remain poorly understood due to the difficulty in studying these interactions in mammalian models. While these findings indicate potential communication of the external microbiome with the developing embryo or fetus, the molecular processes underpinning the effect of the external microbial environment on development across the whole embryo remains unknown.

In this study, we utilize the mechanistic tractability of zebrafish (*Danio rerio*) to test the hypothesis that the external microbiome communicates with the developing embryo and alters the developmental trajectory of the host. Although microbes are too large to directly enter the developing embryo, we posit smaller bioactive microbial-produced molecules, such as metabolites, traverse chorionic pores and drive molecular processes within the embryo, influencing development. We employ a non-targeted approach and perform RNA sequencing

and proteomics on whole embryos at 32hpf raised germ-free (GF) and conventionalized with microbes at 6 hours post-fertilization (hpf) (CV6) and 24hpf (CV24) to identify molecular pathways influenced by microbes and investigate whether there is a time-dependent impact of microbial introduction on development. Our transcriptomic and proteomic results reveal microbes in the surrounding environment communicate with developing embryonic cells, influencing energy metabolism, neurodevelopment, and xenobiotic metabolism. Furthermore, we link microbial-driven transcription to physiological outcomes of embryonic mitochondrial function and later-life larval behavior in the presence of a xenobiotic exposure, demonstrating the microbial community is critical for both embryonic development and developmental responses to xenobiotics.

2. Results

2.1. The External Microbial Community Drives Transcription in the Developing Embryo

To determine if the presence of the external microbial community and the timing of microbial introduction influences molecular processes critical to embryonic development, we generated three groups. First, a complete germ free (GF) group was created by treating zebrafish embryos to remove the commensal microbial community. Two other groups were created by conventionalizing embryos with microbes immediately following the sterilization step at 6 hpf (CV6) or 24hpf (CV24). At 32hpf, embryos were pooled, flash frozen, and extracted RNA was sequenced for transcriptomic analysis. Differential gene expression using DESeq2 (Love et al., 2014; Zhu et al., 2019) revealed a total of 602 genes were significantly differentially expressed (adjusted [adj.] p-value<0.05, Log_2Fold Change>|1|) across all pairwise comparisons. Of these 602 differentially expressed genes (DEGs), 456 were differentially expressed in GF compared to CV24 embryos, the greatest of all comparisons. 237 DEGs were identified in GF compared to CV6 embryos, with 114 of these genes shared with the GF and CV24 comparison. Only 82 genes were differentially expressed between CV24 and CV6 embryos, the fewest of any comparison (Figure 1A). Volcano plots were used to visualize the distribution of DEGs and illustrate the varying magnitude of fold change across each pairwise comparison (Supplemental F1). The CV6 and GF comparison had the greatest variability of fold change while the CV6 and CV24 comparison possessed the least variability in fold change among all pairwise comparisons.

A principal component analysis (PCA) revealed distinct clustering across treatments based on gene expression. Normalized transcript counts for the top 500 most variable transcripts were included in the PCA. Two principal components (PC) were extracted, with PC1 and PC2 describing 34% and 28% of the variance, respectfully, representing a combined total of 62% variance (Figure 1B). The distinct clusters of the GF, CV24, and CV6 treatments demonstrate both microbial colonization status and conventionalization timing effect transcriptional profiles of the developing embryo.

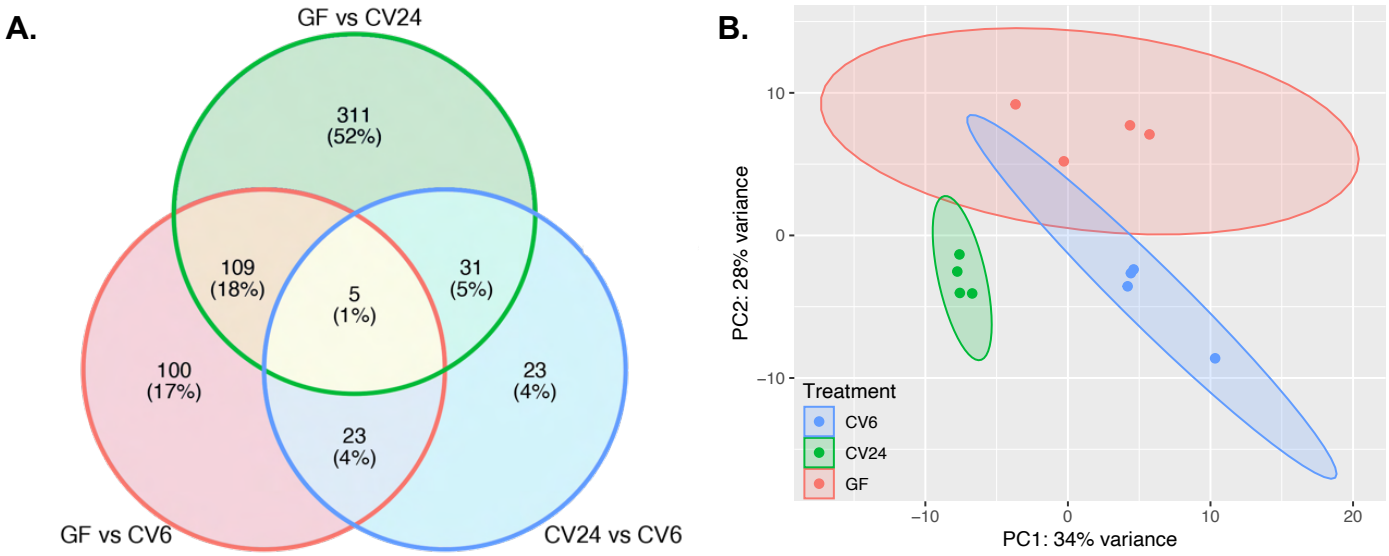

Figure 1. Significant DEGs from DESeq2 pairwise comparisons (adj. p-value<0.05 and Log_2FC>|1|). **(A)** Venn diagram of unique and overlapping DEGs across pairwise comparisons. Top value illustrates the number of DEGs and value in parenthesis indicates the percentage of DEGs compared to the total number of DEGs. **(B)** PCA plot of DESeq2 normalized transcript counts. Top 500 most variable counts included in analysis. Each point

represents a sequenced sample containing 15 pooled embryos at 32hpf. Each condition is represented by 4 sequenced replicates and labeled by treatment condition for CV6 (blue), CV24 (green), and GF (pink).

2.2. The External Microbiome Drives Embryonic Transcription of Energy Metabolism and Neurodevelopment Genes

Four distinct trends in gene expression across CV6, CV24, and GF treatments were identified among the top 1000 significant DEGs analyzed by the DESeq2 LRT command. Of those four gene expression clusters, group 1 consisted of 306 DEGs universally upregulated in CV6 and CV24 samples compared to GF samples and group 2 consisted of 621 DEGs consistently increased among GF samples relative to CV6 and CV24 samples (Figure 2, Supplemental T1). Combined, groups 1 and 2 represent 927 of the top 1000 DEGs, suggesting the presence of a microbial community was the major driver of gene expression, regardless of directionality.

Group 3 was represented by 17 DEGs and group 4 contained 56 DEGs that displayed decreased and increased expression in CV6 embryos, respectively, compared to all other CV24 and GF samples (Figure 2, Supplemental T1). These groups represent the remaining 73 DEGs sensitive to the developmental timepoint at which microbial colonization occurs. These 73 DEGs are only observed to be under transcriptional control by microbes when embryos are conventionalized immediately following sterilization, with no change in expression from GF embryos when conventionalization occurred at 24hpf. It is worth noting, among the top 1000 DEGs, no DEGs shared the same trend in GF and CV6 samples and possessed an opposite trend in CV24 samples. This confirms expression of all top 1000 DEGs was driven by either microbial colonization status or the timing of conventionalization.

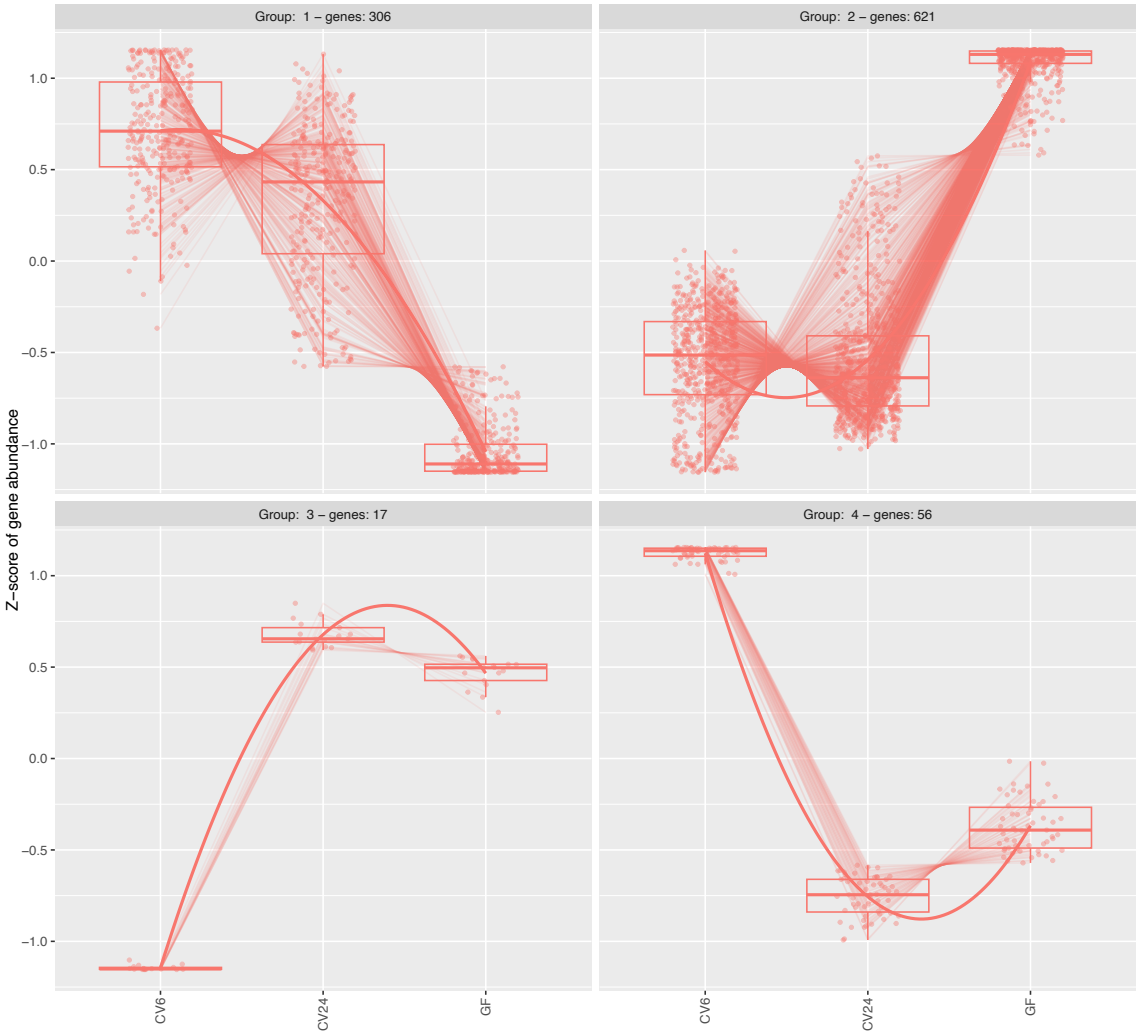

Figure 2. Gene expression patterns identified within the top 1000 DEGs identified by the DESeq2 LRT command across treatments (adj. p-value<0.05). Each group illustrates the number of genes with a similar expression pattern identified using DESeq2 DEGpatterns. Each dot represents the mean transcript abundance across all 4 replicates within a treatment for a particular gene and mean transcript counts are scaled by Z-score. Data are displayed by treatment (x-axis) and Z-score of transcript abundance (y-axis).

Hierarchical clustering and gene ontology (GO) analysis identified significantly enriched biological processing pathways within each gene expression cluster (adj. p-value<0.05). The 306 DEGs included in group 1 broadly clustered into five categories of cellular organization, regeneration, and transport; calcium control of neurotransmitter release; axonemal assembly; retinal/photoreceptor differentiation and development; and carbohydrate metabolism (Supplemental F2A). The 621 DEGs involved in group 2 were generalized by biological processing GO terms related to lipid metabolism, organic acid transport, cell adhesion, protein glycosylation, and 'de novo' protein folding (Supplemental F2B). Although only 17 DEGs were identified in group 3, those genes were involved in biological pathways related to developmental metabolic processes, response to stimuli, 'de novo' protein folding, and protein localization to mitochondrion (Supplemental F2C). The 56 DEGs included in group 4 were clustered into five broad biological processes including cellular response to decreased oxygen, protein hydroxylation, receptor signaling, mitochondrial oxidative phosphorylation, and carbohydrate metabolism (Supplemental F2D).

Among the GO pathways identified to be perturbed across treatments, two broad categories critical to early developmental processes dominated or overlapped across gene expression clusters: visual and neurodevelopmental processes and energy metabolism. The four gene expression clusters and the top 100 DEGs (Supplemental F3) were analyzed by pathway analysis and probed for significant DEGs involved in GO terms related to these three categories. Heat maps were used to visualize transcriptional regulation across samples (Figure 3).

We identified 144 genes involved in energy metabolism (Figure 3A). Of these 144 energy metabolism genes, 44 could be attributed to carbohydrate metabolism, 69 to lipid metabolism, and 31 to mitochondrial function. Hierarchical clustering by rows reveals genes involved in carbohydrate metabolism and mitochondrial function were evenly distributed across gene expression trends. Uniquely, all 69 DEGs involved in lipid metabolism were upregulated in GF embryos compared to CV6 or CV24 embryos (Figure 3A). This is attributed to the overwhelming number of lipid metabolism genes belonging to group 2, with no changes in lipid metabolism being observed in the other gene expression clusters.

43 genes involved in visual and neurodevelopmental processes were also identified (Figure 3B). Hierarchical clustering by rows reveals approximately half of these genes are upregulated and the other half are downregulated in GF embryos compared to CV6 and CV24 embryos, while CV24 and CV6 embryos generally show comparable transcript counts.

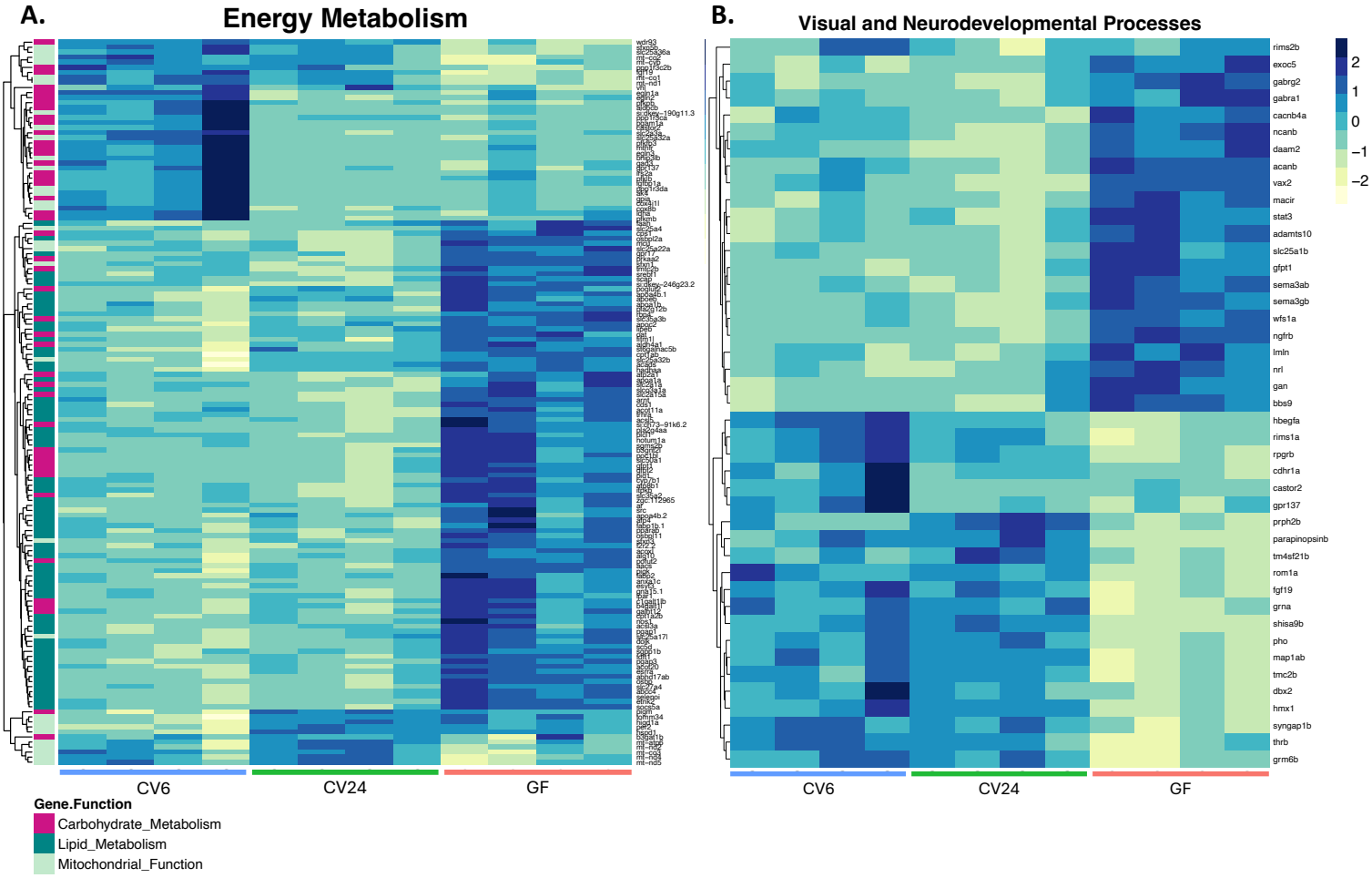

Figure 3. Heatmaps of normalized transcript counts for DEGs involved in **(A)** energy metabolism and **(B)** visual and neurodevelopment. DEGs chosen from significantly enriched pathways (p-value<0.05) identified by hierarchical clustering in gene expression clusters and the top 100 DEGs (Supplemental T3). Transcript counts for each of the 4 sequenced sample replicates per treatment are shown along the x-axis. Each sample is represented by 15 pooled embryos. Counts are scaled by Z-score within rows and gene identifiers are shown on the y-axis.

2.3. The External Microbiome Impacts Embryonic Energy Metabolism and Neurodevelopment Protein Expression

To determine whether the external microbial environment elicited translational effects on the embryonic proteome, an additional subset of CV6, CV24, and GF embryos were pooled, flash frozen, and prepared for protein extraction, digestion, and quantification by LC/MSMS. Differential protein expression using DEP R package (Zhang et al., 2018) revealed a total of 1,146 differentially expressed proteins (p-value<0.05, $Log_2FC>|0.5|$) across all pairwise comparisons. Of the 1,146 differentially expressed proteins (DEP), 492 differed between CV6 and GF embryos, while 469 differed between CV24 and GF embryos, 128 of which overlapped with the CV6 and GF comparison. We identified 575 DEPs between CV6 and CV24 embryos, the greatest of all comparisons, 138 of which overlapped with the CV6 and GF comparison and 128 of which overlapped with the CV24 and GF comparison (Figure 4, Supplemental F4).

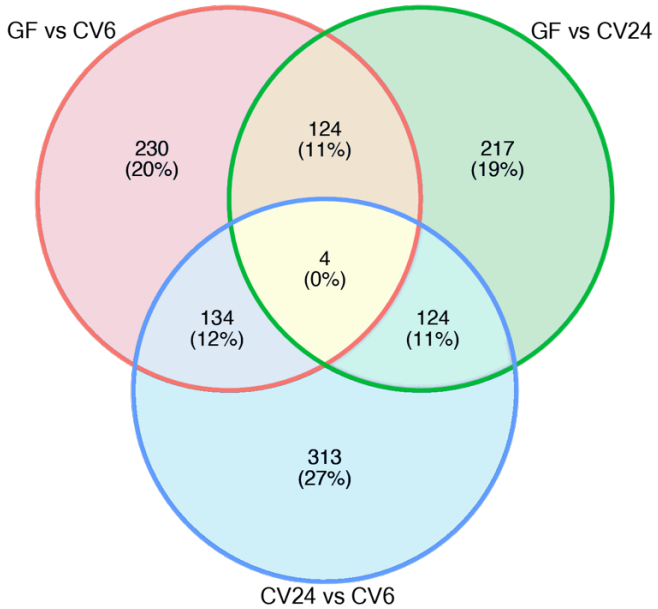

Figure 4. Venn diagram of unique and overlapping DEPs from DEP pairwise comparisons (p-value<0.05 and $Log_2FC>|.05|$). Top value illustrates the number of DEPs and value in parenthesis indicates the percentage of DEPs compared to the total number of DEGs.

To investigate whether the observed transcriptional effects describe the observed differences in protein expression across treatments, we performed pathway analysis on all significant DEPs identified within each pairwise comparison. Pathway analysis revealed a strong signature in proteins related to energy metabolism, particularly those involved in mitochondrial metabolism, organization, and transport across all treatment groups. The CV6 and GF comparison revealed differential expression of proteins involved in the mitochondrial inner membrane, the TCA cycle, Acyl CoA, ATP synthesis, and respiratory electron transport, while the CV24 and GF pairwise comparison revealed differences in the mitochondrial inner membrane, ATPase activity, mitochondrial translation, and phospholipid metabolism. Comparing CV24 and CV6 embryos additionally reveal differential expression of proteins involved in the mitochondrial inner and outer membrane, membrane translocation and protein import, mitochondrial ribosomal subunits and translation, redox cycling, ATP biosynthesis, mitochondrial electron transport chain complex I, oxidative phosphorylation, mTOR signaling, and lipid metabolism. Many of the DEGs identified from the transcriptional dataset encoded for the differentially expressed proteins identified, confirming energy metabolism as a critical embryonic developmental process influenced by the external microbial environment.

While DEPs involved in neurodevelopment were less abundant than those involved in energy metabolism, identified DEPs were consistent with embryonic neurodevelopmental pathways transcriptionally influenced by the external microbial environment. Proteins with differential expression between CV6 and GF embryos are involved in postsynaptic neurons and axonogenesis, while the CV24 and GF pairwise comparison revealed differential proteins involved in neural crest cell differentiation and calcium signaling. The CV24 and CV6 embryos were found to differ in proteins involved in axonogenesis, calcium signaling, and neural crest cell development. Lists of differentially expressed energy metabolism and neurodevelopment proteins identified between each pairwise comparison are included in Supplemental T4.

2.4. The External Microbiome Impacts Bioenergetic and Behavioral Responses to an Embryonic Xenobiotic Exposure

Transcriptomic results further revealed the single most upregulated DEG across all treatments was *cyp1a* (Figure 5) and gene expression trends were confirmed via qPCR (Supplementary F5). Since CYP1A enzyme activity is critical in xenobiotic metabolism via activation of the aryl hydrocarbon receptor (AhR) pathway, we tested whether the influence of the embryonic microbiome on bioenergetic and behavioral responses changed following exposure to a CYP1A agonist. We therefore exposed CV6, CV24, and GF embryos to a potent AhR agonist, benzo(a)pyrene (BaP), or a vehicle control (0.1% dimethyl sulfoxide [DMSO]) at 24hpf throughout the

duration of the experiment and assessed embryonic mitochondrial respiration at 32hpf and larval swimming behavior at 5dpf. BaP is a well-studied neurodevelopmental and mitochondrial toxicant, reported to affect zebrafish bioenergetics and behavior (Hawkey et al., 2022). Our study is the first to reveal the microbiome may impact embryonic responses to BaP exposure.

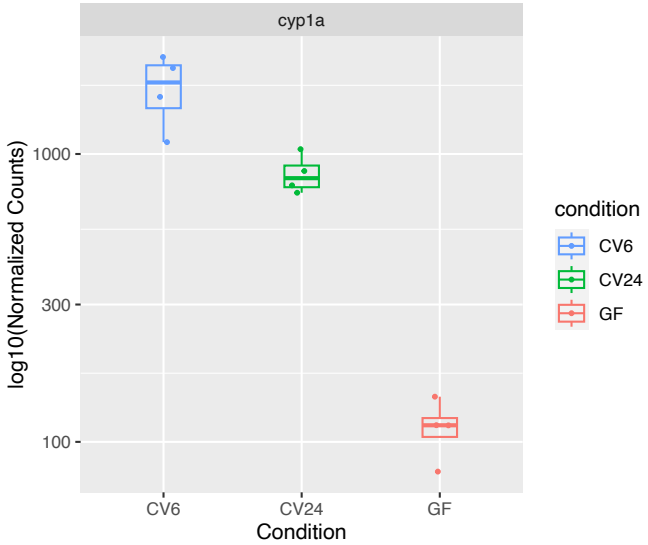

Figure 5. Log_{10} Normalized transcript count for *cyp1a* across CV6, CV24, and GF groups. Each point represents a sequenced sample containing 15 pooled embryos at 32hpf. Each condition is represented by 4 sequenced replicates and labeled by treatment condition for CV6 (blue), CV24 (green), and GF (pink). Data are displayed by microbial treatment (x-axis) and log_{10}(Normalized Counts) (y-axis).

Since transcriptomic results suggest mitochondrial function is altered by the external microbial environment during embryogenesis, mitochondrial respiration was measured in individual whole embryos at 32hpf using a Seahorse BioAnalyzer XFe96 (Agilent Technologies, CA). Our results illustrate no changes in basal or maximal oxygen consumption rates (OCR) occur between microbial treatments in the absence of a BaP exposure (Figure 6). However, a significant decrease in both basal and maximal respiration is observed in CV24 compared to CV6 or GF embryos in the presence of 10μM BaP exposure (Figure 6), while total mitochondrial abundance remains statistically unchanged across treatments (Supplemental F6). This suggests the external microbial community influences embryonic mitochondrial responses to a xenobiotic exposure. No differences in spare capacity or non-mitochondrial respiration were observed across treatments (Supplemental F7).

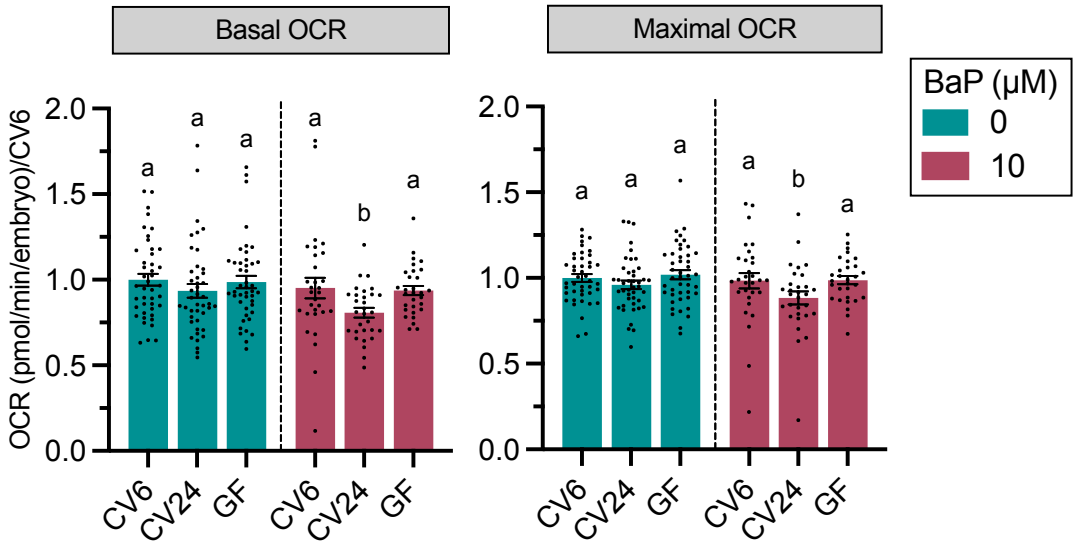

Figure 6. Basal and maximal mitochondrial oxygen consumption rates (OCR) in CV6, CV24, and GF embryos at 32hpf dosed with either a vehicle control (0.1% DMSO) or 10μM BaP. Data normalized to CV6 average.

Significance determined by two 1-way ANOVAs, separated by BaP treatment, Tukey's HSD, $p<0.05$. Error bars represent standard error mean. N=220. Data are displayed by microbial treatment (x-axis), grouped by BaP treatment [0μM BaP (blue) and 10μM BaP (red)], and OCR (pmol/min/embryo), normalized to the average of CV6 (y-axis).

Since transcriptomic results further suggest the microbiome impacts neurodevelopment during embryogenesis, to determine whether early developmental perturbations in neurodevelopmental processes result in a distinct behavioral phenotype in response to BaP exposure during larval development, we performed a behavioral assay on CV6, CV24, and GF larvae with and without BaP exposure at 5dpf. We assessed total distance moved during alternating light and dark cycles using DanioVision™ (Noldus, Wageningen, The Netherlands) and EthoVision XT13 software (Noldus, Wageningen, The Netherlands). Our results indicate larvae raised under GF conditions show an increase in total distance traveled across all light and dark phases compared to CV6 larvae, suggesting hyperactive behavior occurs in the absence of a microbial community during early development (Figure 7). However, CV24 larvae were not statistically different from either CV6 or GF larvae and exhibited minor, but not statistically significant hyperactivity compared to CV6 larvae (Figure 7). Assessing total distance moved across the course of the experiment illustrates the hyperactivity observed in GF larvae is driven by activity in both the light and dark phases (Supplemental F8A). Interestingly, in the presence of an embryonic 10μM BaP exposure, total distance moved in both the CV24 and GF groups significantly increases compared to CV6 larvae, suggesting the presence of a microbial community and timing of conventionalization is important for the behavioral response to BaP (Figure 7). Further analyzing larval distance traveled by minute illustrates GF larvae experience hyperactivity in both the light and dark phases, while CV24 larvae only experience hyperactivity in the dark phase in response to a 10μM BaP exposure (Supplemental F8B).

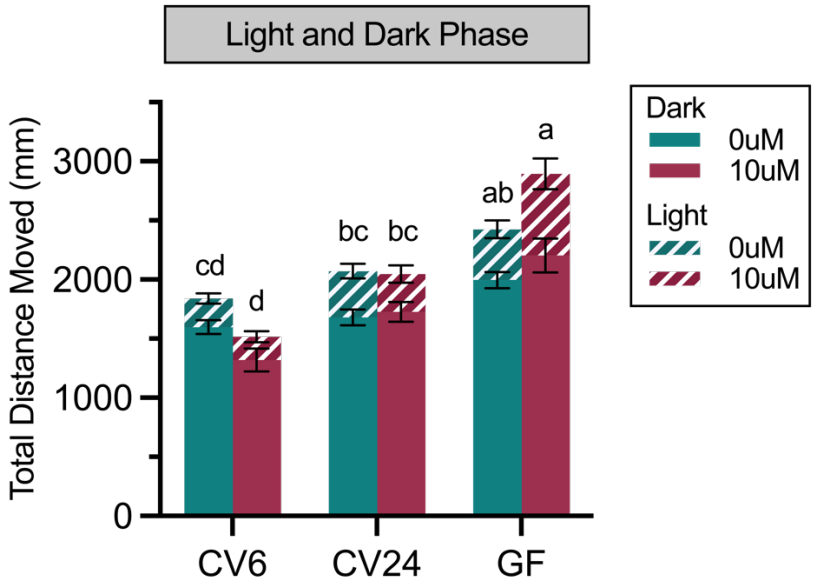

Figure 7. Total distance moved over two sets of alternating 10-minute light/dark cycles in CV6, CV24, and GF larvae at 5dpf dosed with either a vehicle control (0μM BaP; 0.1% DMSO) or 10μM BaP. Data are calculated as the average sum of total distance moved within each treatment across all light and dark phases. 2-way ANOVA, Tukey's HSD, $p<0.05$. Error bars represent standard error mean. N=389. Data are displayed by microbial treatment (x-axis) and total distance moved (mm) (y-axis). Each condition is labeled by BaP treatment (0μM – blue, 10μM – red) and distance moved in light or dark phases (Dark – solid bar, Light – Striped bar).

To assess whether there is a developmental requirement of *cyp1a* activation by microbes, we included 2 additional timepoints of conventionalization, 12hpf (CV12) and 30hpf (CV30) and compared *cyp1a* expression in CV6, CV12, CV24, CV30, and GF embryos at 32hpf using qPCR. Our results confirm *cyp1a* expression is decreased in GF embryos and increased in the presence of a microbial community, regardless of the timing of conventionalization (Supplemental F5).

3. Discussion

3.1. Overview of Differentially Expressed Genes

Overall, our findings highlight a distinct interaction between the external microbial environment and the developing zebrafish embryo, in contrast to the previously held notion that in zebrafish and other oviparous organisms, embryos are shielded from the external microbial environment prior to hatching. Through pairwise analysis of differential expression, we revealed gene expression is more conserved between CV6 and CV24 embryos compared to GF embryos (Figure 1). In our study, this illustrates the presence of the external microbial community has the largest impact on gene transcription, while the timing of conventionalization (6hpf or 24hpf) has a comparatively smaller impact on transcriptional response. In the experiments presented, the CV6 treatment group served as a control, void of a microbial community for the shortest possible duration for our procedures. Immediately following completion of the derivation, microbes were re-introduced to CV6 embryos for the remainder of the experiment. The inclusion of the CV24 treatment aimed to assess whether the absence of a microbial community during the first 24 hours of development affected gene expression, highlighting critical early-life development genes sensitive to the microbial community. Although it was expected the CV6 and GF comparison would have more significant DEGs than the CV24 and GF comparison, the larger distribution of variance in experimental replicates across the CV6 group likely contributes to fewer DEGs observed with significance within the CV6 and GF comparison (Figure 1).

Clustering of gene expression patterns revealed among the top 1000 DEGs, 927 were driven by the presence or absence of a microbiome. Regardless of directionality, gene expression trends across this subset of DEGs were shared between CV24 and CV6 treatments, but significantly different in GF treatments (Figure 2, Supplemental T1). The remaining 73 DEGs exhibited distinct expression in CV6 treatments, with similar expression between CV24 and GF treatments (Figure 2, Supplemental T1). This suggests these 73 genes may be especially sensitive to microbial-driven transcription during the first 24 hours of zebrafish development. However, future studies are required to determine whether expression can be corrected by later reintroduction of the microbiome or if these patterns persist in the absence of a microbial community during the first 24 hours of development.

3.2. The External Microbiome Impacts Embryonic Energy Metabolism

Pathway analysis of gene expression clusters uncovered genes involved in energy metabolism are dependent on both colonization status and the timing of conventionalization (Figure 3A). Among the 144 identified energy metabolism DEGs, a majority exhibited upregulation in GF conditions compared to embryos conventionalized at both 6 and 24 hpf and were involved in in ADP/ATP metabolism and transport, AMPK activity, mitochondrial transmembrane transport, and lipid metabolism (Supplemental F2B, T2). Fewer DEGs were downregulated in GF compared to other groups, encompassing genes involved in carbohydrate metabolism, mitochondrial transmembrane transport, and TORC1 signaling (Supplemental F2A, T2). Genes involved in mitochondrial respiration, mitochondrial organization, mitochondrial membrane permeabilization, ADP/ATP/AMP metabolism, carbohydrate metabolism, and response to reactive oxygen species were differentially regulated in both CV24 and GF compared to CV6 embryos (Supplemental F2C, F2D, T2), suggesting these genes and developmental processes may be sensitive to the external microbial community during the first 24hpf. Pathway analysis of differentially expressed proteins confirmed pathways involved in mitochondrial membrane transport, ATP metabolism, mitochondrial respiration, mTOR signaling, and lipid metabolism differ across treatment groups, further supporting differential regulation of embryonic energy metabolism by the external microbial environment prior to hatching (Supplemental T4).

Previous studies utilizing germ-free models illustrate in the absence of a microbiome, individuals elevate glucose intake and energy production, but experience decreased energy utilization efficiency, although these are findings from larval development (Rawls et al., 2004; Sheng et al., 2018). Our findings are in concordance with these prior observations, but are the first to demonstrate these microbial-directed effects on energy production begin as early as embryogenesis. We demonstrate an upregulation in *slc2a1a* in GF embryos. This gene encodes for a solute carrier involved in glucose transport, suggesting in the absence of a microbiome, carbohydrate transport may increase in response to a heightened energy demand during embryogenesis. A possible mechanism in which the microbiome may indirectly mediates glucose homeostasis is through bile acid metabolism (Kuipers et al., 2014; Ridlon et al., 2014; Utzschneider et al., 2016). Some bile acids serve as ligands for nuclear farnesoid X receptor (FXR), a regulator of fibroblast growth factor-19 (fgf-19), a hormone that

ultimately modulates glucose tolerance through insulin-independent mechanisms (Kuipers et al., 2014; Maliha & Guo, 2021; Sayin et al., 2013; Schaap, 2012). Our results illustrate upregulation of *fgf-19* in CV6 and CV24 embryos compared to GF embryos, suggesting a possible mechanism by which the external microbial environment exerts control over carbohydrate homeostasis during embryogenesis.

Other studies suggest the observed energy deprivation in GF individuals is linked to microbial-modulation of mitochondrial function. Microbial metabolites can impact mitochondrial respiration, biogenesis, oxidative stress, oxidative phosphorylation, the TCA cycle, ATP production, proton leak, and AMPK activity (Clark & Mach, 2017; Donohoe et al., 2011; Frye et al., 2016; Ribeiro et al., 2020; Rose et al., 2018). In the absence of microbial metabolites during post-embryonic development, oxidative phosphorylation and ATP levels decrease while AMPK activity increases, effects which can be reversed by supplementation with butyrate (Donohoe et al., 2011). Our results confirm an increase in *prkaa2* in GF embryos compared to CV24 and CV6 embryos, suggesting GF embryos may compensate for decreased energy utilization efficiency by enhancing glucose uptake, mitochondrial fatty acid oxidation, and respiratory capacity through AMPK-dependent mechanisms (Clark & Mach, 2017; Mollica et al., 2017). While mitochondrial content was observed to remain consistent regardless of the presence of a microbiome (Supplemental F6), we observe an increase in *bnip3lb* only in CV6 embryos, implying these individuals are better equipped to induce mitophagy for proper removal of damaged mitochondria, stimulating increased turnover of mitochondria. This process may contribute to improved energy efficiency in the presence of a microbial environment during early embryogenesis (Pickles et al., 2018; Wrighton et al., 2021).

Our results confirm an interaction between cytochrome c oxidase genes and proteins with the microbial environment, demonstrating a decrease in gene expression of *cox4i1l* and *cox8b* in GF and CV24 compared to CV6 embryos, along with a decrease in protein expression of COX16 in GF embryos and COX6b2 in CV24 embryos (Supplemental F9). This trend was observed previously in larval development, while our results are the first to suggest electron transfer through the electron transport chain is sensitive to microbial conventionalization during the first 24hpf during embryogenesis.

Despite the profound changes in expression levels of genes and proteins associated with cellular energy metabolism, we observed little differences in mitochondrial respiration across treatments. This difference only became pronounced in the presence of a xenobiotic exposure. With exposure to BaP, CV24 embryos showed an overall reduction of both basal and maximal mitochondrial respiration compared to CV6 and GF embryos. This suggests the microbiome is increasingly important during the first 24 hours of development to maintain mitochondrial respiration rates in response to a xenobiotic exposure and is further explained by the observed decrease in cytochrome c oxidase genes. However, it is unclear why neither basal nor maximal mitochondrial respiration were observed to decrease in GF embryos in response to a BaP exposure at 32hpf. It is possible GF embryos may have sufficient time to reach metabolic homeostasis in the absence of microbially directed cues. In contrast, CV24 embryos received microbial directed cues, although developmentally later than CV6 embryos and, as a result, may readjust mitochondrial respiration efficiency.

While this adaptive response to a lack of microbiome may potentially explain the uniform increase in lipid metabolism genes in GF embryos, it is still unclear why cytochrome c oxidase genes maintain decreased expression in GF embryos. Further investigation is needed to understand the mechanisms by which GF embryos maintain mitochondrial respiration rates during embryogenesis in response to a BaP exposure and to determine whether embryos conventionalized at 24hpf can recover mitochondrial respiration efficiency to the level of CV6 embryos. Regardless, mitochondrial respiration was measured at 32hpf, prior to embryonic hatching from the chorion. If the conventional notion that pre-hatched embryos are shielded from the external microbial environment held true, there would be no observable differences across microbial treatments when exposed to BaP. Therefore, the observed decrease in respiration rates in CV24 embryos upon exposure to BaP provides additional support to the importance of microbial-directed cues on energy metabolism as early as embryogenesis.

As mentioned, all 68 DEGs identified to be involved in lipid metabolism were uniformly upregulated within GF embryos (Figure 3A). Germ-free studies during post-embryonic development suggest cholesterol synthesis and mitochondrial fatty acid oxidation increase under GF conditions (Brown et al., 2023; Lickwar et al., 2022; Rawls et al., 2004; Sheng et al., 2018), while fatty acid synthesis, absorption, transport, and accumulation increase under conventionalized conditions (Brown et al., 2023; Clark & Mach, 2017; Lickwar et al., 2022; Semova et al., 2012; Sheng et al., 2018). Our results support an increase in fatty acid oxidation and cholesterol synthesis in GF embryos, possibly as a compensatory attempt to increase energy production in the absence of microbial directed cues. However, contradictory to previous studies, we observe upregulation of genes related to lipid synthesis, absorption, and transport under GF conditions, results that could be attributed to the timing of sampling (Supplemental F2, T2). To our knowledge, this study is the first to explore the impacts of the microbiome

on lipid metabolism during embryogenesis. It is possible in the absence of a microbiome during early development, lipid synthesis is initially upregulated, and subsequently downregulated as energy storage becomes depleted. However, further studies are needed to investigate the mechanisms in which energy dynamics shift in the absence of microbial directed cues during embryonic development.

3.3. The External Microbiome Impacts Embryonic Neurodevelopment

Our results additionally reveal visual and neurodevelopmental processes are influenced by the external microbial environment during early development, regardless of conventionalization timing. A majority of these 43 DEGs display similar transcript counts in CV6 and CV24 embryos, with significantly different expression in GF embryos (Figure 3B). Our findings demonstrate the differential regulation of genes involved in aspects of embryonic neurodevelopment including calcium control of neurotransmitter release and synaptic transmission, retinal/photoreceptor cell differentiation and development, glial cell/neuron differentiation and development, and swimming behavior, among several others (Supplemental F2, T2). Our proteomic analysis confirms differential expression of proteins involved in these pathways, including calcium signaling, post-synaptic transmission, axonogenesis, and neural progenitor cell differentiation and development (Supplemental T4), supporting neurodevelopment as a critical process sensitive to microbial cues during embryonic development.

Many of these pathways have been studied previously in the context of microbial regulation during post-embryonic development, including calcium and neurotransmitter signaling, synaptic plasticity, visual development, axonogenesis, and HPA/HPI axis activation (Davis et al., 2016; Heijtz et al., 2011; Kaur et al., 2023; Massaquoi et al., 2023; Rea et al., 2022; Vuong et al., 2020). However, less is known regarding the microbial regulation of these pathways during embryonic development. Our findings support a model in which the external microbial environment influences the regulation of critical neurodevelopment pathways prior to hatching. Utilizing a mouse model, Vuong et al. (2020) demonstrated the maternal microbiome modulates fetal neurodevelopment, resulting in post-natal behavioral effects. This study discovered axonogenesis was reduced during embryogenesis in offspring from microbiome depleted dams, marked by differential expression of several genes, including GABA receptor genes *gabra1* and *gabrg2* (Vuong et al., 2020). Similarly, our study observed differential regulation of genes and proteins related to axonogenesis, including increases in *gabra1* and *gabrg2* and decreases in p21 protein (Cdc42/Rac)-activated kinase 1 and 2a (PAK1 and PAK2a) (Supplemental T4). Although conducted in a mammalian species lacking a protective chorionic structure during development, this study aligns with our results, collectively demonstrating the role of the microbiome in development commences prenatally during embryogenesis, a developmental timepoint largely overlooked in microbiome studies.

Findings from Rea et al. (2022) align with our results, suggesting a delay in neurodevelopment under GF conditions. Rea et al. (2022) further demonstrated these effects could be rescued by the addition of specific microbes or their metabolites. While our study shows both upregulation and downregulation of neurodevelopmental genes in the presence of microbes, pathway analysis revealed the most significant impact on neurodevelopment in gene expression cluster group 1, including genes downregulated in GF embryos compared to CV24 and CV6. Furthermore, Rea et al. (2022) suggest GF embryos experience dysregulated eye and lens development, Wnt signaling, and neuron and glial organization. Our results confirm disruption of eye and lens development and neurogenesis, although the specific DEGs involved in these processes differed between the two studies. The variance in identified DEGs may be attributed to differences in collection timing or methods employed in pathway analysis. Our transcriptomic analysis was conducted at 32hpf, while Rea et al. (2022) investigated differences at 48hpf. Some DEGs were additionally noted to not appear until after hatching, suggesting timing of collection may play a role (Rea et al., 2022). While dysregulated Wnt signaling pathways fell outside our significance cutoff for pathway analysis ($p\text{-value}<0.05$) and were not included in our analysis, individual genes involved in Wnt signaling were significantly differentially regulated in our study. Collectively, these studies support a role for the external microbial community in proper neurodevelopment during embryogenesis, although further research is needed to elucidate the mechanisms involved and understand the potential long-term outcomes of this microbial requirement.

Our behavioral observations are among the first to investigate the later-life outcomes of microbial colonization during embryogenesis. Our results indicate embryonic transcriptional and translational differences play a role in shaping larval behavioral responses, as we show hyperactivity in GF larvae compared to CV6 larvae that were conventionalized as embryos. Furthermore, we demonstrate a time-dependent impact of conventionalization, as CV24 embryos conventionalized at 24hpf display mild hyperactivity, but not to the extent of GF embryos. However, while differences in swimming behavior between CV6 and CV24 larvae are not statistically significant in the absence of a BaP treatment, a time-dependent impact of conventionalization

becomes evident upon exposure to BaP. When exposed to BaP, both GF and CV24 larvae display hyperactivity compared to CV6 embryos conventionalized earlier during development. This further emphasizes the significance of the external microbial community during the first 24 hours of development in regulating behavioral responses to xenobiotic exposure. Previous studies have established individuals raised under germ-free conditions experience hyperactivity and disruptions in anxiety-like behaviors compared to individuals raised under conventionalized conditions (Catron et al., 2019; Davis et al., 2016; Heijtz et al., 2011; Phelps et al., 2017), and furthermore, that microbiota impacts neurodevelopmental toxicity of xenobiotics (Catron et al., 2019). However, to our knowledge, this is the first study to suggest the presence of an external microbiome during embryogenesis and the *timing* of introduction is significant for larval behavioral outcomes and behavioral response to xenobiotics, suggesting a direct influence of the external microbial environment on neurodevelopment during embryogenesis.

4. Conclusion

The role of the microbiome in shaping organismal fitness is abundantly clear and the current data effectively demonstrate this influence commences as early as embryogenesis. We demonstrate the presence of the external microbial community and the timing of conventionalization impacts embryonic energy metabolism (carbohydrate metabolism, lipid metabolism, mitochondrial function), visual and neurodevelopment, as well as energetic and behavioral responses to a potent xenobiotic, benzo(a)pyrene. This knowledge transforms our approach to germ-free studies, particularly in the context of embryonic developmental studies, and challenges current beliefs that embryos develop completely shielded from the microbial environment until after hatching. Further studies will aim to elucidate the molecular drivers of microbial communication during early-life development through biochemical profiling to identify specific microbial products or bacterial species driving the observed responses. This work will ultimately expand understanding of host-microbe interactions during the earliest and most sensitive stages of vertebrate development, providing a foundation to examine the role of the microbiome in developmental origins of metabolic and neurological disorders as well as developmental effects of *in utero* chemical exposures in a human health context. Current findings are of particular significance to developmental plasticity of oviparous organisms and their overall ecological fitness in microbially dynamic natural habitats.

5. Methods

5.1. Zebrafish husbandry

Adult conventionally raised Ekkwill zebrafish were maintained in a recirculating AHAB system at 24-28°C on a 14:10 h light/dark cycle at Duke University. Adults were placed in breeder tanks (3 females, 2 males) with dividers overnight. When the lights turned on in the morning, breeding pairs were transferred to new breeder tanks containing freshly made artificial seawater (ASW; 0.8g/L Instant Ocean, 0.12g/L sodium bicarbonate, pH 7.0-8.0, 28°C). Adults were left to breed for approximately one hour before embryos were collected.

5.2. Germ-free Derivation and Conventionalization

Germ-free derivation was performed as previously described (Pham et al., 2008). Briefly, embryos were collected in 25mL of sterile antibiotic solution (AB) containing 0.2-µm sterile filtered 30% Danieau's medium (1.06 g/L NaCl, 16.3 mg/L KCl, 15 mg/L $MgSO_4$, 31 mg/L $Ca(NO_3)_2$, 375 mg/L HEPES, pH 7.6)**,** 250ng/mL amphotericin B, 10µg/mL kanamycin, and 100µg/mL ampicillin. Fertilized embryos were sorted and transferred into an additional 25mL of AB in a 50mm sterile petri dish, with no more than 50 embryos per 25mL. Petri dishes were incubated at 28°C for 4 hours and developing embryos in the sphere stage were selected and transferred to a sterile 15mL conical tube. The following steps were then performed in a laminar flow hood to ensure sterility. Embryos were washed 3 times with AB, exposed to a 0.05% polyvinylpyrrolidone solution for 2 minutes, rinsed 3 times with sterile 30% Danieau's, exposed to 0.005% sodium hypochlorite for 20 minutes, and rinsed 3 times with sterile 30% Danieau's. Groups of 25 germ-free (GF) embryos were then transferred to 25-cm^2 cell culture flasks containing 25mL of sterile 30% Danieau's and reared in a 28°C incubator. At 24hpf, 80% of the volume in each flask was replaced with sterile Danieau's. Sterility of GF flasks is confirmed every 24 hours by plating 40uL embryo medium on a tryptic soy agar (TSA) plates and culturing for at least 6 days at 28°C.

Conventionalized (CV) embryos simultaneously underwent germ-free treatment and were subsequently conventionalized by performing an 80% water change and replacing 50% of sterile embryo medium with AHAB system water, creating a microbial concentration of 10^3 colony forming units/mL (Pham et al., 2008; Tan et al., 2019), which was confirmed by plating the conventionalized medium on TSA plates and assessing bacterial growth after 24 hours at 28°C. Conventionalization with system water was performed immediately following derivation at 6hpf and at 24hpf, to generate treatments CV6 and CV24, respectively.

5.3. RNA Extraction, Library Preparation, and Sequencing

15 embryos from each CV6, CV24, or GF treatment were selected at 32hpf, pooled, and flash frozen on liquid nitrogen for RNA sequencing. RNA was extracted from each pooled sample of embryos using RNeasy® QIAGEN Mini Kit (74104, QIAGEN Inc.) according to manufacture instructions. RNA concentration and quality was analyzed using NanoDrop and samples were aliquoted and stored at -80°C. Library preparation and sequencing were performed on embryos across 4 experimental replicates by Duke University Sequencing and Genomic Technologies. Briefly, 200ng RNA was used to generate KAPA mRNA HyperPrep (Roche) whole-transcriptome libraries. RNA was captured with magnetic oligo-dT beads and fragmented at 94°C for 2 minutes. Libraries were barcoded using Illumina Dual Index Adapters and amplified by PCR for 14 cycles. Amplified libraries were then pooled and the Illumina NovaSeq 6000 system was used for 50 base pair paired-end sequencing.

5.4. Sequence Processing

Paired-end sequenced reads were processed as previously described (Pertea et al., 2016) using the Duke University high-powered Computing Cluster. Briefly, Illumina TruSeq3-PE adapters and low quality reads (Q<20) were trimmed using Trimomatic v0.39 (Bolger et al., 2014). The zebrafish reference genome was downloaded from Ensembl (GRCz11, Ensembl 110, GCA_000002035.4) (Martin et al., 2023) and extracted splice sites and exons were used to create an index using HISAT2 v2.2.0 (Kim et al., 2019). Trimmed paired-end reads were mapped and aligned to the indexed zebrafish reference genome using HISAT2. Generated SAM files were then sorted, converted to BAM format, and sequencing lanes merged using Samtools v1.10 (Danecek et al., 2021). Merged alignments were assembled into full-length transcripts and quantified using StringTie v2.2.1 (Pertea et al., 2015). The python scriplet 'prepDE.py3' (http://ccb.jhu.edu/software/stringtie/dl/prepDE.py3) with the '-e' option was used to generate readable counts of transcript abundances. Transcript counts were filtered to include only those with a total >10 reads.

5.5. Differential Gene Expression Analysis

Differential gene expression analysis was performed using R (v4.3.2) and Bioconductor (v3.18) packages DESeq2 (v1.42.0) (Love et al., 2014; Zhu et al., 2019) and DEGreport (v1.38.5) (Pantano, 2023). Bioconductor package org.Dr.eg.db (v3.18.0) (Carlson, 2019) was used to annotate zebrafish gene names. Pairwise comparisons between each treatment group were performed using the Wald test with an adj. p-value<0.05. The LRT command from DESeq2 with an adj. p-value<0.05 was used to compare all three treatment groups and identify interactions between conventionalization status and timing of conventionalization. Results from the LRT were used to identify significantly enriched pathways.

RNAseq DEGs from each pairwise comparisons were graphed in a Venn Diagram using CRAN package ggVennDiagram (v1.2.3) (Gao et al., 2021) and in volcano plots using Bioconductor (v3.18) package EnhancedVolcano (v1.20.0) (Blighe et al., 2018) with an adj. p-value<0.05 and Log_2Fold Change>|1| used as thresholds to subset the data and determine significance. A principal component analysis (PCA) was performed with the top 500 most variable RNAseq transcript counts across all treatment groups. Transcript counts were variance stabilized and graphed with plotPCA function of DESeq2 using default parameters.

5.6. Gene Expression Trends and Hierarchical Clustering of Enriched GO Terms

The top 1000 significant RNAseq DEGs identified by the DESeq2 LRT command were regular log transformed and the degPatterns function of the DEGreport package (v1.38.5) (Pantano, 2023) was used to identify gene expression trends across sample groups using default parameters. Genes within each gene expression trend cluster were extracted and the enrichGO function of the ClusterProfiler package (v4.11.0) (Wu

et al., 2021; Yu et al., 2012) was used to identify enriched biological processing pathways using default parameters. Pathways with a p-value<0.05 were considered significant and included in analysis. Treeplots of enriched pathways were created using Enrichplot (v1.22.0) (Yu, 2023) functions.

5.7. Heatmaps of Differential Gene Expression

RNAseq transcript counts were normalized using a variance stabilizing transformation using DESeq2. Normalized counts were scaled by Z-score and graphed using CRAN package pheatmap (v1.0.12) (Kolde, 2018). Genes involved in energy metabolism and visual and neurodevelopmental processes were selected from significantly enriched pathways identified by the enrichGO function of the ClusterProfiler package (v4.11.0) (Wu et al., 2021; Yu et al., 2012) across the 4 gene expression clusters as well as genes included in the top 100 DEGs (Supplemental F3).

5.8. Xenobiotic Exposure

To determine whether the external microbial environment impacted embryonic responses to a xenobiotic exposure, CV6, CV24, and GF embryos were raised as previously described. At 24hpf, embryos were aqueously exposed to 10μM benzo(a)pyrene (Sigma-Aldrich, CAS 50-32-8) in dimethyl sulfoxide (DMSO), or a 0.1% DMSO vehicle control and raised in exposure media under GF or conventionalized conditions until endpoint collection.

5.9. Mitochondrial Function Assays

To determine if differences in mitochondrial metabolism could physiologically be observed across treatments, CV6, CV24, and GF whole embryos at 32hpf, exposed to BaP (10μM) or a vehicle control (0.1% DMSO), were assessed for mitochondrial respiration rate using the Seahorse BioAnalyzer XFe96 (Agilent Technologies, CA) according to previously published protocol (Babich et al., 2020; Souders et al., 2018). Oxygen consumption rate (OCR) measurements were made per individual embryo. Embryos were first screened to ensure no developmental deformities were selected for assay and then placed in the center of separate spheroid chambers at the bottom of individual wells in a spheroid microplate containing 150ul of sterile (GF) or conventionalized (CV24 or CV6) Danieau's medium. OCR was measured by the Seahorse BioAnalyzer at basal levels and following the injection of electron transport chain inhibitors. Maximal mitochondrial respiration was measured following the injection of 6μM carbonyl cyanide-p-trifluoromethoxyphenylhydrazone (FCCP) (Sigma-Aldrich, CAS 370-86-5) and non-mitochondrial respiration was measured following injection of 6.25mM sodium azide (Sigma- Aldrich, CAS 26628-22-8). Basal OCR was measured for 8 cycles, post-injection of FCCP was measured for 8 cycles, and post-injection of sodium azide was measured for 35 cycles, with a 1 minute mix, 1 minute wait, and 2 minute measure per cycle. Assays were repeated across three experimental replicates.

Following each run, non-mitochondrial OCR was identified as the minimum OCR measurement after sodium azide injection, basal OCR was calculated as the last measurement prior to FCCP injection minus non-mitochondrial OCR, maximal OCR was the maximum measurement following FCCP injection minus non-mitochondrial OCR, and spare capacity was calculated by subtracting basal OCR from maximal OCR. Values for each embryo were calculated individually and normalized across experiments to the average of CV6 embryos within each experiment. Values that fell outside ±1.5(IQR) based on a standard normal distribution were excluded from data analysis and the remaining individuals within treatments were averaged. Two one-way ANOVAs, separated by BaP dose, with Tukey post-hoc tests, were used to determine significance (p-value<0.05) between CV6, CV24, and GF treatments with and without BaP exposure.

5.10. Larval Behavioral Assays

To determine if neurological dysfunction from colonization status during early embryonic development resulted in alterations in swimming behavior later during larval development, CV6, CV24, and GF embryos, exposed to BaP (10μM) or a vehicle control (0.1% DMSO), were raised under GF or conventionalized conditions until 5dpf. At 5dpf, locomotor response during light-dark cycles was measured using DanioVision™ (Noldus, Wageningen, The Netherlands). Larvae were first screened to ensure no developmental deformities were selected for assay, randomly selected, and transferred into individual wells of a clear, flat-bottom 96-well plate with approximately 200uL of either sterile (GF) or conventionalized (CV6 and CV24) Danieau's, depending on the media used for that treatment. Assays were repeated across three experimental replicates.

The location of the larvae in each well was recorded every 0.016 seconds using EthoVision XT13 (Noldus, Wageningen The Netherlands) software during a 10 minute habituation period in the dark, followed by 2 cycles of 10 minute light followed by 10 minute dark, for a total of a 50 minutes per assay. Total distance traveled was measured by mm/minute based on the recorded larval location during each light or dark phase. Values that fell outside ±1.5(IQR) based on a standard normal distribution were excluded from data analysis and the remaining individuals within treatments were averaged. Total distance traveled was analyzed for significance using a two-way ANOVA with a Tukey post-hoc test (p-value<0.05).

5.11. Proteomic Sample Preparation, and Quantitative LC-MS/MS Analysis

Fifteen embryos from each CV6, CV24, or GF treatment were selected at 32hpf, pooled, flash frozen on liquid nitrogen, and kept at -80ºC until protein extraction. Sample preparation and protein quantification was performed on embryos across 4 experimental replicates by Duke University Proteomics and Metabolomics Core Facility. Briefly, samples were probe sonicated in 5% SDS and total protein content was quantified using a Bradford Assay. 20µg of extracted protein from each sample was reduced with 10 mM DTT at 80°C for 10 min, alkylated with 25 mM iodoacetamide for 30 min at 21ºC, and 1.2% phosphoric acid and 200µl of S-Trap (Protifi) binding buffer (90% MeOH/100mM TEAB) were added to each sample for denaturation. Proteins were bound to the S-Trap micro cartridge, digested with 80 ng/µL trypsin (Promega) at 47°C for 1 hour, and eluted by adding 50 mM TEAB, 0.2% FA, and 50% ACN/0.2% FA. Samples were lyophilized and resuspended in 20µl of 1% TFA/2% MeCN. An equal volume of each sample was combined to produce a quality control for the study design.

1µl of each sample was analyzed in a randomized order by Quantitative LC/MSMS on a Vanquish Neo UHPLC coupled to a Thermo Orbitrap Astral. Samples were bound to a PepMap C18 0.3 mm x 5 mm column and separated with a 150µm ID x 8 cm, 1.5µm (PepSep) column using increasing concentration of 5 to 30% acetonitrile with 0.1% formic acid for 30 minutes at 55 °C. Data was retrieved using a data-independent acquisition (DIA) mode. DIA data were converted to .htrms format and processed in Spectronaut 18 (18.7.240325.55695 Biognosys). A spectral library was built for zebrafish using a NCBI database and a tryptic specificity up to 2. Protein groups were filtered by a 1% peptide and protein false-discovery rate, used for local normalization (Callister et al., 2006), and protein abundances were calculated using the MaxLFQ algorithm (Cox et al., 2014).

5.12. Differential Protein Expression Analysis

Differential protein expression analysis was performed using R (v4.3.2) and Bioconductor (v3.18) package DEP (v1.26.0) (Zhang et al., 2018). Data were filtered for proteins identified in at least 3 out of 4 replicates of at least one condition using a threshold value of 1 in the filter_missval command. Normalization of the filtered data was compared to non-normalized data, which revealed a variance stabilizing transformation produced right-skewed dataset (Supplemental F10). Therefore, since the non-normalized filtered data appeared to follow a more Gaussian distribution, non-normalized data were used for further analysis. A comparison of all significant proteins (adjusted [adj.] p-value<0.05) and the fold change of tested pairwise comparisons for normalized and non-normalized data is include in Supplemental F11. Missing values were determined to be random (MAR) and therefore a k-nearest neighbor approach with a rowmax of 0.9 was used to impute missing values. Pairwise comparisons between each treatment group were performed based on linear models and empirical Bayes statistics. Significant differentially expressed proteins were identified by a p-value<0.05 and a Log_2Fold Change>|0.5| (Supplemental T5). DEPs from each pairwise comparison were graphed in a Venn Diagram using CRAN package ggVennDiagram (v1.2.3) (Gao et al., 2021) and a principal component analysis was performed with the top 500 most variable protein counts across all treatment groups and graphed with plot_PCA function of DEP using default parameters.

Significantly differentially expressed proteins (p-value<0.05, Log_2Fold Change>|0.5|) from each pairwise comparison were analyzed for pathway analysis using DAVID (Huang et al., 2009; Sherman et al., 2022). Energy metabolism and neurodevelopmental pathways with a p-value<0.05 were considered significant and the names of these individual proteins are included in Supplementary T3.

5.13. cDNA Synthesis and quantitative PCR (qPCR)

In order to determine whether the timing of conventionalization influenced *cyp1a* gene expression, CV and GF embryos were generated using the methods defined above, including different timepoints of

conventionalization. Germ free embryos were conventionalized with the same concentration of zebrafish AHAB system water at 6hpf (CV6), 12hpf (CV12), 24hpf (CV24), and 30hpf (CV30). 15 embryos from each treatment were selected at 32hpf, pooled, flash frozen on liquid nitrogen, and stored at -80°C until sample processing. All experiments were repeated 3 times. RNA was extracted from each pooled sample using RNeasy® QIAGEN Mini Kit (74104, QIAGEN Inc.) according to manufacture instructions and RNA concentration and quality was confirmed using a NanoDrop UV-Vis Spectrophotometer (Thermo Fisher Scientific, Inc.). Extracted RNA was diluted to 150ng/µl and 15µl per sample were added to a well containing 2µl 10x RT buffer, 0.8µl 100mM dNTPs, 2µl 10x random primers, 1µl reverse transcriptase (MultiScribe), 1µl RNase inhibitor, and 3.2µl nuclease-free water (Applied Biosystems™ 4374966). cDNA was then generated on a thermocycler under the following reaction conditions: 25°C for 10 minutes, 37°C for 2 hours, and 85°C for 5 minutes, and stored at -80°C. cDNA was diluted to 3ng/µl and 2µl per sample were added to a well containing 10µl Luna Universal Probe qPCR Master Mix (New England Biolabs, M3004), 1.6µl forward/reverse *cyp1a* primer, 0.4µl *cyp1a* probe, 0.8µl forward/reverse *actb1* primer, 0.2µl *actb1* probe, and 5µl nuclease-free water. Primers and probes were provided by IDT (Integrated DNA Technologies, Inc.), sequence properties and off-target compatibility was assessed using SciTools™ OligoAnalyzer™ Tool (PrimerQuest™ Program, IDT, Coralville, Iowa, USA. Accessed 15 May, 2024. Https://Www.Idtdna.Com/SciTools), and sequences are included in Supplemental T6. Transcript abundance was quantified via quantitative-PCR (qPCR) on a Analytik Jena qTower^3 (Analytik Jena, Germany) under the following reaction conditions: 95°C for 120 seconds, with 45 cycles of 95°C for 15 seconds and 52°C for 60 seconds. *Actb1* was used as the housekeeping reference gene and relative transcript abundance of *cyp1a* was quantified using the ΔΔCt method, normalizing to the average of CV6 replicates. Primer efficiencies were calculated at 103% and 109% for *cyp1a* and *actb1*, respectfully.

References

Babich, R., Ulrich, J. C., Ekanayake, E. M. D. V., Massarsky, A., De Silva, P. M. C. S., Manage, P. M., Jackson, B. P., Ferguson, P. L., Di Giulio, R. T., Drummond, I. A., & Jayasundara, N. (2020). Kidney developmental effects of metal-herbicide mixtures: Implications for chronic kidney disease of unknown etiology. *Environment International*, *144*(August), 106019. https://doi.org/10.1016/j.envint.2020.106019

Benkendorff, K., Davis, A. R., & Bremner, J. B. (2001). Chemical Defense in the Egg Masses of Benthic Invertebrates: An Assessment of Antibacterial Activity in 39 Mollusks and 4 Polychaetes. *Journal of Invertebrate Pathology*, *78*(2), 109–118. https://doi.org/10.1006/jipa.2001.5047

Bertotto, L. B., Catron, T. R., & Tal, T. (2020). Exploring interactions between xenobiotics, microbiota, and neurotoxicity in zebrafish. *NeuroToxicology*, *76*, 235–244. https://doi.org/10.1016/j.neuro.2019.11.008

Blighe, K., Rana, S., & Lewis, M. (2018). *EnhancedVolcano: Publication-ready volcano plots with enhanced colouring and labeling.* (1.20.0) [Computer software]. https://github.com/kevinblighe/EnhancedVolcano

Bolger, A. M., Lohse, M., & Usadel, B. (2014). Trimmomatic: A flexible trimmer for Illumina sequence data. *Bioinformatics*, *30*(15), 2114–2120. https://doi.org/10.1093/bioinformatics/btu170

Brown, A., Goldsworthy, S. M., Barnes, A. A., Eilert, M. M., Tcheang, L., Daniels, D., Muir, A. I., Wigglesworth, M. J., Kinghorn, I., Fraser, N. J., Pike, N. B., Strum, J. C., Steplewski, K. M., Murdock, P. R., Holder, J. C., Marshall, F. H., Szekeres, P. G., Wilson, S., Ignar, D. M., … Dowell, S. J. (2003). The Orphan G Protein-coupled Receptors GPR41 and GPR43 Are Activated by Propionate and Other Short Chain Carboxylic Acids. *Journal of Biological Chemistry*, *278*(13), 11312–11319. https://doi.org/10.1074/jbc.M211609200

Brown, E. M., Clardy, J., & Xavier, R. J. (2023). Gut microbiome lipid metabolism and its impact on host physiology. *Cell Host & Microbe*, *31*(2), 173–186. https://doi.org/10.1016/j.chom.2023.01.009

Callister, S. J., Barry, R. C., Adkins, J. N., Johnson, E. T., Qian, W.-J., Webb-Robertson, B.-J. M., Smith, R. D., & Lipton, M. S. (2006). Normalization approaches for removing systematic biases associated with mass spectrometry and label-free proteomics. *Journal of Proteome Research*, *5*(2), 277–286. https://doi.org/10.1021/pr050300l

Carlson, M. (2019). *org.Dr.eg.db: Genome wide annotation for Zebrafish* (3.8.2) [R package].

Catron, T. R., Gaballah, S., & Tal, T. (2019). Using Zebrafish to Investigate Interactions Between Xenobiotics and Microbiota. *Current Pharmacology Reports*, *5*(6), 468–480. https://doi.org/10.1007/s40495-019-00203-7

Catron, T. R., Swank, A., Wehmas, L. C., Phelps, D., Keely, S. P., Brinkman, N. E., McCord, J., Singh, R., Sobus, J., Wood, C. E., Strynar, M., Wheaton, E., & Tal, T. (2019). Microbiota alter metabolism and mediate neurodevelopmental toxicity of 17β-estradiol. *Scientific Reports*, *9*(1), 7064. https://doi.org/10.1038/s41598-019-43346-9

Chen, Z.-Y., Li, N.-J., Cheng, F.-Y., Hsueh, J.-F., Huang, C.-C., Lu, F.-I., Fu, T.-F., Yan, S.-J., Lee, Y.-H., & Wang, Y.-J. (2020). The Effect of the Chorion on Size-Dependent Acute Toxicity and Underlying Mechanisms of Amine-Modified Silver Nanoparticles in Zebrafish Embryos. *International Journal of Molecular Sciences*, *21*(8), 2864. https://doi.org/10.3390/ijms21082864

Cholan, P. M., Han, A., Woodie, B. R., Watchon, M., Kurz, A. R., Laird, A. S., Britton, W. J., Ye, L., Holmes, Z. C., McCann, J. R., David, L. A., Rawls, J. F., & Oehlers, S. H. (2020). Conserved anti-inflammatory effects and sensing of butyrate in zebrafish. *Gut Microbes*, *12*(1), 1824563. https://doi.org/10.1080/19490976.2020.1824563

Clark, A., & Mach, N. (2017). The crosstalk between the gut microbiota and mitochondria during exercise. *Frontiers in Physiology*, *8*(MAY). https://doi.org/10.3389/fphys.2017.00319

Cox, J., Hein, M. Y., Luber, C. A., Paron, I., Nagaraj, N., & Mann, M. (2014). Accurate proteome-wide label-free quantification by delayed normalization and maximal peptide ratio extraction, termed MaxLFQ. *Molecular & Cellular Proteomics : MCP*, *13*(9), 2513–2526. https://doi.org/10.1074/mcp.M113.031591

Danecek, P., Bonfield, J. K., Liddle, J., Marshall, J., Ohan, V., Pollard, M. O., Whitwham, A., Keane, T., McCarthy, S. A., Davies, R. M., & Li, H. (2021). Twelve years of SAMtools and BCFtools. *GigaScience*, *10*(2), giab008. https://doi.org/10.1093/gigascience/giab008

Davis, D. J., Bryda, E. C., Gillespie, C. H., & Ericsson, A. C. (2016). Microbial modulation of behavior and stress responses in zebrafish larvae. *Behavioural Brain Research*, *311*, 219–227. https://doi.org/10.1016/j.bbr.2016.05.040

De La Paz, J. F., Anguita-Salinas, C., Díaz-Celis, C., Chávez, F. P., & Allende, M. L. (2020). The Zebrafish Perivitelline Fluid Provides Maternally-Inherited Defensive Immunity. *Biomolecules*, *10*(9), 1274. https://doi.org/10.3390/biom10091274

Den Besten, G., Van Eunen, K., Groen, A. K., Venema, K., Reijngoud, D.-J., & Bakker, B. M. (2013). The role of short-chain fatty acids in the interplay between diet, gut microbiota, and host energy metabolism. *Journal of Lipid Research*, *54*(9), 2325–2340. https://doi.org/10.1194/jlr.R036012

Donohoe, D. R., Garge, N., Zhang, X., Sun, W., O'Connell, T. M., Bunger, M. K., & Bultman, S. J. (2011). Microbiome, The Regulate, Butyrate Metabolism, Energy. *Cell Metabolism*, *13*(5), 517–526. https://doi.org/10.1016/j.cmet.2011.02.018.The

Flórez, L. V., Biedermann, P. H. W., Engl, T., & Kaltenpoth, M. (2015). Defensive symbioses of animals with prokaryotic and eukaryotic microorganisms. *Natural Product Reports*, *32*(7), 904–936. https://doi.org/10.1039/C5NP00010F

Frye, R. E., Rose, S., Chacko, J., Wynne, R., Bennuri, S. C., Slattery, J. C., Tippett, M., Delhey, L., Melnyk, S., Kahler, S. G., & MacFabe, D. F. (2016). Modulation of mitochondrial function by the microbiome metabolite propionic acid in autism and control cell lines. *Translational Psychiatry*, *6*(10), 1–10. https://doi.org/10.1038/tp.2016.189

Gao, C.-H., Yu, G., & Cai, P. (2021). ggVennDiagram: An Intuitive, Easy-to-Use, and Highly Customizable R Package to Generate Venn Diagram. *Frontiers in Genetics*, *12*, 706907. https://doi.org/10.3389/fgene.2021.706907

Gao, Z., Yin, J., Zhang, J., Ward, R. E., Martin, R. J., Lefevre, M., Cefalu, W. T., & Ye, J. (2009). Butyrate Improves Insulin Sensitivity and Increases Energy Expenditure in Mice. *Diabetes*, *58*(7), 1509–1517. https://doi.org/10.2337/db08-1637

Gómez, G. D., & Balcázar, J. L. (2008). A review on the interactions between gut microbiota and innate immunity of fish. *FEMS Immunology and Medical Microbiology*, *52*(2), 145–154. https://doi.org/10.1111/j.1574-695X.2007.00343.x

Hamdoun, A., & Epel, D. (2007). Embryo stability and vulnerability in an always changing world. *Proceedings of the National Academy of Sciences*, *104*(6), 1745–1750. https://doi.org/10.1073/pnas.0610108104

Hawkey, A. B., Piatos, P., Holloway, Z., Boyda, J., Koburov, R., Fleming, E., Di Giulio, R. T., & Levin, E. D. (2022). Embryonic exposure to benzo[a]pyrene causes age-dependent behavioral alterations and long-term metabolic dysfunction in zebrafish. *Neurotoxicology and Teratology*, *93*, 107121. https://doi.org/10.1016/j.ntt.2022.107121

Heijtz, R. D., Wang, S., Anuar, F., Qian, Y., Björkholm, B., Samuelsson, A., Hibberd, M. L., Forssberg, H., & Pettersson, S. (2011). Normal gut microbiota modulates brain development and behavior. *Proceedings of the National Academy of Sciences of the United States of America*, *108*(7), 3047–3052. https://doi.org/10.1073/pnas.1010529108

Huang, D. W., Sherman, B. T., & Lempicki, R. A. (2009). Systematic and integrative analysis of large gene lists using DAVID bioinformatics resources. *Nature Protocols*, *4*(1), 44–57. https://doi.org/10.1038/nprot.2008.211

Kaur, N., LaForce, G., Mallela, D. P., Saha, P. P., Buffa, J., Li, X. S., Sangwan, N., Rothenberg, K., & Zhu, W. (2023). Exploratory Transcriptomic Profiling Reveals the Role of Gut Microbiota in Vascular Dementia. *International Journal of Molecular Sciences*, *24*(9), 8091. https://doi.org/10.3390/ijms24098091

Kellner, R. L. L. (2002). Molecular identification of an endosymbiotic bacterium associated with pederin biosynthesis in Paederus sabaeus (Coleoptera: Staphylinidae). *Insect Biochemistry and Molecular Biology*, *32*(4), 389–395. https://doi.org/10.1016/S0965-1748(01)00115-1

Kellner, R. L. L., & Dettner, K. (1996). Differential efficacy of toxic pederin in deterring potential arthropod predators of Paederus (Coleoptera: Staphylinidae) offspring. *Oecologia*, *107*(3), 293–300. https://doi.org/10.1007/BF00328445

Kim, D., Paggi, J. M., Park, C., Bennett, C., & Salzberg, S. L. (2019). Graph-based genome alignment and genotyping with HISAT2 and HISAT-genotype. *Nature Biotechnology*, *37*(8), 907–915. https://doi.org/10.1038/s41587-019-0201-4

Kimura, I., Ozawa, K., Inoue, D., Imamura, T., Kimura, K., Maeda, T., Terasawa, K., Kashihara, D., Hirano, K., Tani, T., Takahashi, T., Miyauchi, S., Shioi, G., Inoue, H., & Tsujimoto, G. (2013). The gut microbiota suppresses insulin-mediated fat accumulation via the short-chain fatty acid receptor GPR43. *Nature Communications*, *4*(1), 1829. https://doi.org/10.1038/ncomms2852

Kolde, R. (2018). *Pheatmap* (1.0.12) [CRAN].

Kuipers, F., Bloks, V. W., & Groen, A. K. (2014). Beyond intestinal soap—Bile acids in metabolic control. *Nature Reviews Endocrinology*, *10*(8), 488–498. https://doi.org/10.1038/nrendo.2014.60

Lickwar, C. R., Davison, J. M., Kelly, C., Mercado, G. P., Wen, J., Davis, B. R., Tillman, M. C., Semova, I., Andres, S. F., Vale, G., McDonald, J. G., & Rawls, J. F. (2022). Transcriptional Integration of Distinct Microbial and Nutritional Signals by the Small Intestinal Epithelium. *Cellular and Molecular Gastroenterology and Hepatology*, *14*(2), 465–493. https://doi.org/10.1016/j.jcmgh.2022.04.013

Love, M. I., Huber, W., & Anders, S. (2014). Moderated estimation of fold change and dispersion for RNA-seq data with DESeq2. *Genome Biology*, *15*(12), 550. https://doi.org/10.1186/s13059-014-0550-8

MacFabe, D. F. (2012). Short-chain fatty acid fermentation products of the gut microbiome: Implications in autism spectrum disorders. *Microbial Ecology in Health & Disease*, *23*(0). https://doi.org/10.3402/mehd.v23i0.19260

Maliha, S., & Guo, G. L. (2021). Farnesoid X receptor and fibroblast growth factor 15/19 as pharmacological targets. *Liver Research*, *5*(3), 142–150. https://doi.org/10.1016/j.livres.2021.02.002

Martin, C. R., Osadchiy, V., Kalani, A., & Mayer, E. A. (2018). The Brain-Gut-Microbiome Axis. *Cellular and Molecular Gastroenterology and Hepatology*, *6*(2), 133–148. https://doi.org/10.1016/j.jcmgh.2018.04.003

Martin, F. J., Amode, M. R., Aneja, A., Austine-Orimoloye, O., Azov, A. G., Barnes, I., Becker, A., Bennett, R., Berry, A., Bhai, J., Bhurji, S. K., Bignell, A., Boddu, S., Branco Lins, P. R., Brooks, L., Ramaraju, S. B., Charkhchi, M., Cockburn, A., Da Rin Fiorretto, L., … Flicek, P. (2023). Ensembl 2023. *Nucleic Acids Research*, *51*(D1), D933–D941. https://doi.org/10.1093/nar/gkac958

Martín-Vivaldi, M., Soler, J. J., Peralta-Sánchez, J. M., Arco, L., Martín-Platero, A. M., Martínez-Bueno, M., Ruiz-Rodríguez, M., & Valdivia, E. (2014). Special structures of hoopoe eggshells enhance the adhesion of symbiont-carrying uropygial secretion that increase hatching success. *Journal of Animal Ecology*, *83*(6), 1289–1301. https://doi.org/10.1111/1365-2656.12243

Massaquoi, M. S., Kong, G. L., Chilin-Fuentes, D., Ngo, J. S., Horve, P. F., Melancon, E., Hamilton, M. K., Eisen, J. S., & Guillemin, K. (2023). Cell-type-specific responses to the microbiota across all tissues of the larval zebrafish. *Cell Reports*, *42*(2), 112095. https://doi.org/10.1016/j.celrep.2023.112095

McFall-Ngai, M., Hadfield, M. G., Bosch, T. C. G., Carey, H. V., Domazet-Lošo, T., Douglas, A. E., Dubilier, N., Eberl, G., Fukami, T., Gilbert, S. F., Hentschel, U., King, N., Kjelleberg, S., Knoll, A. H., Kremer, N., Mazmanian, S. K., Metcalf, J. L., Nealson, K., Pierce, N. E., … Wernegreen, J. J. (2013). Animals in a bacterial world, a new imperative for the life sciences. *Proceedings of the National Academy of Sciences*, *110*(9), 3229–3236. https://doi.org/10.1073/pnas.1218525110

Mollica, M. P., Mattace Raso, G., Cavaliere, G., Trinchese, G., De Filippo, C., Aceto, S., Prisco, M., Pirozzi, C., Di Guida, F., Lama, A., Crispino, M., Tronino, D., Di Vaio, P., Berni Canani, R., Calignano, A., & Meli, R. (2017). Butyrate Regulates Liver Mitochondrial Function, Efficiency, and Dynamics in Insulin-Resistant Obese Mice. *Diabetes*, *66*(5), 1405–1418. https://doi.org/10.2337/db16-0924

Neis, E., Dejong, C., & Rensen, S. (2015). The Role of Microbial Amino Acid Metabolism in Host Metabolism. *Nutrients*, *7*(4), 2930–2946. https://doi.org/10.3390/nu7042930

Pantano, L. (2023). *DEGreport: Report of DEG analysis* (1.38.5) [R Package].

Pelzer, E., Gomez-Arango, L. F., Barrett, H. L., & Nitert, M. D. (2017). Review: Maternal health and the placental microbiome. *Placenta*, *54*, 30–37. https://doi.org/10.1016/j.placenta.2016.12.003

Pertea, M., Kim, D., Pertea, G. M., Leek, J. T., & Salzberg, S. L. (2016). Transcript-level expression analysis of RNA-seq experiments with HISAT, StringTie and Ballgown. *Nature Protocols*, *11*(9), 1650–1667. https://doi.org/10.1038/nprot.2016.095

Pertea, M., Pertea, G. M., Antonescu, C. M., Chang, T.-C., Mendell, J. T., & Salzberg, S. L. (2015). StringTie enables improved reconstruction of a transcriptome from RNA-seq reads. *Nature Biotechnology*, *33*(3), 290–295. https://doi.org/10.1038/nbt.3122

Pham, L. N., Kanther, M., Semova, I., & Rawls, J. F. (2008). Methods for generating and colonizing gnotobiotic zebrafish. *Nature Protocols*, *3*(12), 1862–1875. https://doi.org/10.1038/nprot.2008.186

Phelps, D., Brinkman, N. E., Keely, S. P., Anneken, E. M., Catron, T. R., Betancourt, D., Wood, C. E., Espenschied, S. T., Rawls, J. F., & Tal, T. (2017). Microbial colonization is required for normal neurobehavioral development in zebrafish. *Scientific Reports*, *7*(1), 1–13. https://doi.org/10.1038/s41598-017-10517-5

Pickles, S., Vigié, P., & Youle, R. J. (2018). Mitophagy and Quality Control Mechanisms in Mitochondrial Maintenance. *Current Biology*, *28*(4), R170–R185. https://doi.org/10.1016/j.cub.2018.01.004

PrimerQuest™ program, IDT, Coralville, Iowa, USA. Accessed 15 May, 2024. Https://www.idtdna.com/SciTools. (n.d.).

Rawls, J. F., Samuel, B. S., & Gordon, J. I. (2004). Gnotobiotic zebrafish reveal evolutionarily conserved responses to the gut microbiota. *Proceedings of the National Academy of Sciences of the United States of America*, *101*(13), 4596–4601. https://doi.org/10.1073/pnas.0400706101

Rawson, D. M., Zhang, T., Kalicharan, D., & Jongebloed, W. L. (2000). Field emission scanning electron microscopy and transmission electron microscopy studies of the chorion, plasma membrane and syncytial layers of the gastrula-stage embryo of the zebrafish Brachydanio rerio: A consideration of the structural and functional: EM studies of gastrula-stage zebrafish embryos *D M Rawson* et al *. Aquaculture Research*, *31*(3), 325–336. https://doi.org/10.1046/j.1365-2109.2000.00401.x

Rea, V., Bell, I., Ball, T., & Van Raay, T. (2022). Gut-derived metabolites influence neurodevelopmental gene expression and Wnt signaling events in a germ-free zebrafish model. *Microbiome*, *10*(1), 132. https://doi.org/10.1186/s40168-022-01302-2

Ribeiro, M. F., Santos, A. A., Afonso, M. B., Rodrigues, P. M., Sá Santos, S., Castro, R. E., Rodrigues, C. M. P., & Solá, S. (2020). Diet-dependent gut microbiota impacts on adult neurogenesis through mitochondrial stress modulation. *Brain Communications*, *2*(2). https://doi.org/10.1093/braincomms/fcaa165

Ridlon, J. M., Kang, D. J., Hylemon, P. B., & Bajaj, J. S. (2014). Bile acids and the gut microbiome: *Current Opinion in Gastroenterology*, *30*(3), 332–338. https://doi.org/10.1097/MOG.0000000000000057

Rose, S., Bennuri, S. C., Davis, J. E., Wynne, R., Slattery, J. C., Tippett, M., Delhey, L., Melnyk, S., Kahler, S. G., MacFabe, D. F., & Frye, R. E. (2018). Butyrate enhances mitochondrial function during oxidative stress in cell lines from boys with autism. *Translational Psychiatry*, *8*(1). https://doi.org/10.1038/s41398-017-0089-z

Sampson, T. R., & Mazmanian, S. K. (2015). Control of Brain Development, Function, and Behavior by the Microbiome. *Cell Host & Microbe*, *17*(5), 565–576. https://doi.org/10.1016/j.chom.2015.04.011

Sayin, S. I., Wahlström, A., Felin, J., Jäntti, S., Marschall, H.-U., Bamberg, K., Angelin, B., Hyötyläinen, T., Orešič, M., & Bäckhed, F. (2013). Gut Microbiota Regulates Bile Acid Metabolism by Reducing the Levels of Tauro-beta-muricholic Acid, a Naturally Occurring FXR Antagonist. *Cell Metabolism*, *17*(2), 225–235. https://doi.org/10.1016/j.cmet.2013.01.003

Schaap, F. G. (2012). Role of fibroblast growth factor 19 in the control of glucose homeostasis: *Current Opinion in Clinical Nutrition and Metabolic Care*, *15*(4), 386–391. https://doi.org/10.1097/MCO.0b013e3283547171

Semova, I., Carten, J. D., Stombaugh, J., MacKey, L. C., Knight, R., Farber, S. A., & Rawls, J. F. (2012). Microbiota regulate intestinal absorption and metabolism of fatty acids in the zebrafish. *Cell Host and Microbe*, *12*(3), 277–288. https://doi.org/10.1016/j.chom.2012.08.003

Sheng, Y., Ren, H., Limbu, S. M., Sun, Y., Qiao, F., Zhai, W., Du, Z. Y., & Zhang, M. (2018). The presence or absence of intestinal microbiota affects lipid deposition and related genes expression in zebrafish (Danio rerio). *Frontiers in Microbiology*, *9*(MAY), 1–9. https://doi.org/10.3389/fmicb.2018.01124

Sherman, B. T., Hao, M., Qiu, J., Jiao, X., Baseler, M. W., Lane, H. C., Imamichi, T., & Chang, W. (2022). DAVID: a web server for functional enrichment analysis and functional annotation of gene lists (2021 update). *Nucleic Acids Research*, *50*(W1), W216–W221. https://doi.org/10.1093/nar/gkac194

Silva, Y. P., Bernardi, A., & Frozza, R. L. (2020). The Role of Short-Chain Fatty Acids From Gut Microbiota in Gut-Brain Communication. *Frontiers in Endocrinology*, *11*, 25. https://doi.org/10.3389/fendo.2020.00025

Souders, C. L., Liang, X., Wang, X., Ector, N., Zhao, Y. H., & Martyniuk, C. J. (2018). High-throughput assessment of oxidative respiration in fish embryos: Advancing adverse outcome pathways for mitochondrial dysfunction. *Aquatic Toxicology*, *199*, 162–173. https://doi.org/10.1016/j.aquatox.2018.03.031

Tan, F., Limbu, S. M., Qian, Y., Qiao, F., Du, Z.-Y., & Zhang, M. (2019). The Responses of Germ-Free Zebrafish (Danio rerio) to Varying Bacterial Concentrations, Colonization Time Points, and Exposure Duration. *Frontiers in Microbiology*, *10*, 2156. https://doi.org/10.3389/fmicb.2019.02156

Utzschneider, K. M., Kratz, M., Damman, C. J., & Hullarg, M. (2016). Mechanisms Linking the Gut Microbiome and Glucose Metabolism. *The Journal of Clinical Endocrinology & Metabolism*, *101*(4), 1445–1454. https://doi.org/10.1210/jc.2015-4251

Venema, K. (2010). Role of gut microbiota in the control of energy and carbohydrate metabolism: *Current Opinion in Clinical Nutrition and Metabolic Care*, *13*(4), 432–438. https://doi.org/10.1097/MCO.0b013e32833a8b60

Vuong, H. E., Pronovost, G. N., Williams, D. W., Coley, E. J. L., Siegler, E. L., Qiu, A., Kazantsev, M., Wilson, C. J., Rendon, T., & Hsiao, E. Y. (2020). The maternal microbiome modulates fetal neurodevelopment in mice. *Nature*, *586*(7828), 281–286. https://doi.org/10.1038/s41586-020-2745-3

Wang, H., Ji, D., Shao, J., & Zhang, S. (2012). Maternal transfer and protective role of antibodies in zebrafish Danio rerio. *Molecular Immunology*, *51*(3–4), 332–336. https://doi.org/10.1016/j.molimm.2012.04.003

Wang, Z., & Zhang, S. (2010). The role of lysozyme and complement in the antibacterial activity of zebrafish (Danio rerio) egg cytosol. *Fish & Shellfish Immunology*, *29*(5), 773–777. https://doi.org/10.1016/j.fsi.2010.07.002

Wedekind, C. (2016). Additive Genetic Effects on Embryo Viability in a Whitefish (Salmonidae)Influenced by the Water Mould Saprolegnia ferax. *Journal of Bacteriology & Parasitology*, *07*(03). https://doi.org/10.4172/2155-9597.S4-001

Wilkins, L. G. E., Fumagalli, L., & Wedekind, C. (2016). Effects of host genetics and environment on egg-associated microbiotas in brown trout (*Salmo trutta*). *Molecular Ecology*, *25*(19), 4930–4945. https://doi.org/10.1111/mec.13798

Wilkins, L. G. E., Rogivue, A., Schütz, F., Fumagalli, L., & Wedekind, C. (2015). Increased diversity of egg-associated bacteria on brown trout (Salmo trutta) at elevated temperatures. *Scientific Reports*, *5*(1), 17084. https://doi.org/10.1038/srep17084

Wilson, J. G. (1973). *Environment and birth defects*. Academic Press.

Wrighton, P. J., Shwartz, A., Heo, J. M., Quenzer, E. D., LaBella, K. A., Harper, J. W., & Goessling, W. (2021). Quantitative intravital imaging in zebrafish reveals in vivo dynamics of physiological-stress-induced mitophagy. *Journal of Cell Science*, *134*(4), 1–16. https://doi.org/10.1242/jcs.256255

Wu, T., Hu, E., Xu, S., Chen, M., Guo, P., Dai, Z., Feng, T., Zhou, L., Tang, W., Zhan, L., Fu, X., Liu, S., Bo, X., & Yu, G. (2021). clusterProfiler 4.0: A universal enrichment tool for interpreting omics data. *The Innovation*, *2*(3), 100141. https://doi.org/10.1016/j.xinn.2021.100141

Younge, N., McCann, J. R., Ballard, J., Plunkett, C., Akhtar, S., Araújo-Pérez, F., Murtha, A., Brandon, D., & Seed, P. C. (2019). Fetal exposure to the maternal microbiota in humans and mice. *JCI Insight*, *4*(19), e127806. https://doi.org/10.1172/jci.insight.127806

Yu, G. (2023). *enrichplot: Visualization of Functional Enrichment Result.* (1.22.0) [Computer software].

Yu, G., Wang, L.-G., Han, Y., & He, Q.-Y. (2012). clusterProfiler: An R Package for Comparing Biological Themes Among Gene Clusters. *OMICS: A Journal of Integrative Biology*, *16*(5), 284–287. https://doi.org/10.1089/omi.2011.0118

Zakis, D. R., Paulissen, E., Kornete, L., Kaan, A. M. (Marije), Nicu, E. A., & Zaura, E. (2022). The evidence for placental microbiome and its composition in healthy pregnancies: A systematic review. *Journal of Reproductive Immunology*, *149*, 103455. https://doi.org/10.1016/j.jri.2021.103455

Zhang, X., Smits, A. H., van Tilburg, G. B., Ovaa, H., Huber, W., & Vermeulen, M. (2018). Proteome-wide identification of ubiquitin interactions using UbIA-MS. *Nature Protocols*, *13*(3), 530–550. https://doi.org/10.1038/nprot.2017.147

Zhu, A., Ibrahim, J. G., & Love, M. I. (2019). Heavy-tailed prior distributions for sequence count data: Removing the noise and preserving large differences. *Bioinformatics*, *35*(12), 2084–2092. https://doi.org/10.1093/bioinformatics/bty895